HAL
open science

Grazing Incidence X-ray Diffraction investigation of strains in silicon nanowires obtained by gold catalytic growth

D. Buttard, P. Gentile, Hubert Renevier

To cite this version:

D. Buttard, P. Gentile, Hubert Renevier. Grazing Incidence X-ray Diffraction investigation of strains in silicon nanowires obtained by gold catalytic growth. Surface Science : A Journal Devoted to the Physics and Chemistry of Interfaces, 2011, 605 (5-6), pp.570-576. 10.1016/j.susc.2010.12.019 . hal-01067027

HAL Id: hal-01067027

https://hal.science/hal-01067027

Submitted on 24 Jan 2019

HAL is a multi-disciplinary open access archive for the deposit and dissemination of scientific research documents, whether they are published or not. The documents may come from teaching and research institutions in France or abroad, or from public or private research centers.

L'archive ouverte pluridisciplinaire **HAL**, est destinée au dépôt et à la diffusion de documents scientifiques de niveau recherche, publiés ou non, émanant des établissements d'enseignement et de recherche français ou étrangers, des laboratoires publics ou privés.

Grazing Incidence X-ray Diffraction investigation of strains in silicon nanowires obtained by gold catalytic growth

By *Denis Buttard*, Pascal Gentile*, and *Hubert Renevier*

[*] Prof. D. Buttard, P. Gentile Corresponding-Author, Prof. D. Buttard
Grenoble/INAC/SiNaPS-MINATEC 17 avenue des martyrs
38054 Grenoble, France.
E-mail: denis.buttard@cea.fr
Prof. D. Buttard
Université Joseph Fourier/IUT-1 17 quai C. Bernard
38000 Grenoble, France.
Prof. H. Renevier
Laboratoire des Matériaux et du Génie Physique, G-INP-MINATEC, 3 parvis L. Néel
BP257, 38016 Grenoble 1, France

Keywords: Nanowires, Silicon, Gold catalyst, Grazing Incidence X ray Diffraction

Steady progress has been made in recent years in both the preparation and application of nanostructures. Semi-conductor nanowires in particular have stimulated a lot of interest[1] because of the potential applications in nanotechnology and micro and nano-electronics. One way to prepare semi-conductor nanowires is through the well-known Chemical-Vapor-Deposition (CVD) process in a Vapor-Liquid-Solid (VLS) mode.[2] With this method, the nanowires are grown in catalytic mode, which considerably increases the kinetics of growth and leads to regular crystalline nanowires. The development of this process has made it possible to obtain very good quality crystalline wires, with good self-organisation as well as some radial hetero-junctions. These improvements will enable applications not only for gas sensors and optical detectors[3,4,5] but also for solar cells. For instance, it is possible to produce a solar cell[6] on flexible material composed of a perfect array of *n-type* CdS nanowires embedded in a p-type CdTe layer. Numerous articles have underlined the importance of this development.[7,8,9]

For all these applications, and in order to produce high quality devices, a lot of parameters must be controlled and understood, and in particular that of nanowire structure. This structure is a key element in the process, first from a morphologic point of view, and second in relation

to its transport properties in functional devices. A number of papers have already been published on wire structure based both on experimental investigations using electron microscopy or x-ray techniques[10,11] and on theoretical atomistic models.[12,13] However, although silicon nanowires (SiNW) usually have good crystalline properties, a large variety of wires can still be obtained depending on the growth conditions, and this raises numerous questions. For instance, the role of the early stages of growth on the structure, strain and also stress in wires, is still not really understood. The role of the catalyst in the growth of wires and the strains produced in them has also yet to be investigated.

In this paper, we present experimental results obtained from using x-ray diffraction and electron microscopy on silicon nanowires grown by a VLS catalytic technique. The strain in wires is measured accurately and the role of the gold catalyst in the strains produced is observed and analyzed. A possible origin of the strain is proposed.

Figure 1 shows SEM images from samples after growth in the CVD reactor. It can be seen that the nanostructures obtained result in cylindrical nanowires with high aspect ratio normal to the silicon surface and randomly distributed all over the surface. By varying the duration of growth, we obtain silicon nanowires of several lengths For t = 10 min at T = 650°C and 5 sccm of Silane (SiH_4), the wires have a length of about L = 350 nm (so-called “short” wires (S)) (Figure 1(a)), for t = 15 min at T = 700°C and 10 sccm of Silane, L = 1177 nm (so-called “medium” wires (M)) (Figure 1(b)), and for t = 15 min at T = 575°C and 10 sccm of Silane L = 2782 nm (so-called “long” wires (L)) (Figure 1(c)). The diameter depends on the diameter of the initial gold catalyst and growth results in silicon nanowires with a distribution of diameters ranging from small (d = 30 nm) to large (d = 300 nm).

The shape of nanowires is slightly different depending on the diameter, those with smaller diameters being more cylindrical. In all cases, the wires can be divided into three parts: the foot, the body, and the head. The foot is generally pyramidal (even for small-diameter wires,

but not very easy to observe) which corresponds to equilibrium, which is difficult to obtain in the early stages of growth. From large-resolution images, it can be seen that this foot is composed of large facets with a pyramidal shape. When growth equilibrium is obtained, the wire grows with a more cylindrical shape. From accurate observations of zoom SEM images, we can see that the wire cross-sections may be hexagonal, dodecagonal or polygonal, depending on the experimental conditions of growth.[14] Moreover, each facet is composed of smaller saw-tooth facets with trigonal symmetry. These results have already been published.[15] All the facets show the crystalline character of the wires, and the fact that the direction of growth is normal to the sample surface is evidence that the wires are in epitaxy with the substrate.

The head of wires is composed of a hemispherical droplet. Figure 2 shows a zoom from a typical silicon nanowire head grown in catalytic mode using the VLS method. In Figure 2(a), obtained from a topographic image of SEM using secondary electrons, we can see that the shape is not strictly hemispherical, but slightly flattened. Moreover, the head is composed of two parts, white and dark in colour, indicating variation in the external topography of the droplet. By using backscattered electrons (which correspond to chemical contrast imaging in the SEM) we obtain Figure 2(b). The two parts can be clearly seen again, but this time the white part corresponds to a material of high atomic number (i.e. Au) and the black one to a material of low atomic number (i.e. Si). From careful observation of this image, we can also see that the black part contains very small white parts. In fact, the head of the wires is composed of an alloy, Au/Si, divided into different parts where the percentage of Au/Si varies: the white parts are rich in Au, while the black parts have a low Au content. Previous studies using Transmission Electron Microscopy (TEM) observations[16] have also mentioned the presence of gold clusters on the external surface of the wires, more especially at the top of the wire. It is difficult to observe these clusters with SEM images, but they are nevertheless present.

Before conducting diffraction experiments, we performed X-Ray Reflectivity (XRR) measurements (Figure 3). The reflected intensity is plotted in arbitrary units versus the scattering vector q defined by $q = (4\pi/\lambda)\sin(\alpha_i)$ where α_i is the incident angle. The XRR curve corresponding to the silicon nanowires with gold catalyst is plotted with full circles. For an incident angle lower than the critical angle α_c = 0.15625°of silicon at this wavelength ($\alpha_i < \alpha_c$), we observe the total reflection plateau where the reflected intensity is constant. When the intensity starts to decrease ($\alpha_i = \alpha_c$), we measure $\alpha_c \approx 0.155°$ in agreement with the expected value. For $\alpha_i > \alpha_c$, the intensity strongly decreases and the x-ray beam goes through the substrate. The beam is reflected by the sample and interference fringes appear. A first group of fringes with a small period is observed not far from α_c. By measuring the period Δq, we can estimate the thickness d of the scattering objects with the relation $d = 2\pi/\Delta q$. We measure d = 35 nm. As interference fringes come from the contrast in electronic density between materials, these oscillations are attributed to the presence of gold on the sample. More specifically, the oscillations could come from the hemispherical droplets composing the head of the wires. As previously stated, however, a wide range of diameters, from 30 nm up to 300 nm, is observed on the SEM images. The XRR do not allow observation of all these diameters. Consequently, it may be supposed that in this case the geometry of the experiment only allows observation of small-diameter golden wire heads. For large q, we observe wide thickness fringes, corresponding to a thickness $d \approx 4.3$ nm. SEM images do not reveal nanowires of such small diameter. We believe that these wide thickness fringes come from gold grains that are still present on the silicon surface after annealing and growth. As the conditions of growth were fixed to produce relatively large-diameter nanowires, the very small ones (d < 30 nm) did not grow. Finally, we do not believe that these thickness fringes come from the native silicon oxide layer present on a silicon surface, which usually has a

mean thickness of about 1 to 2 nm. If this were the case, the contrast between the fringes would be less marked.

We then performed Grazing Incident X-Ray Diffraction (GIXD) measurements. Typical diffraction profiles are shown in Figure 4. The diffracted intensity is plotted against the scattering vector q along the in-plane direction <300> (of the hexagonal system) for the <111> oriented silicon wafer. The profile reveals a narrow peak (Sub), arising from diffraction by the silicon substrate, and a broader one (SiNW) attributable to Bragg's diffraction of the silicon nanowires. This observation is evidence of the crystalline character of the wires and of their epitaxy with the silicon substrate. Even if the peak is broader than the substrate, it remains relatively narrow and well defined. There is only a small mosaicity in the wires, and very few defects. Both peaks, (SiNW) and (Sub), have different q values. Consequently, there is a lattice mismatch parameter between the silicon wafer and the silicon nanowires defined by: $\Delta a/a = (a_{SiNW}-a_{Sub})/a_{Sub}$, where a_{SiNW} and a_{Sub} are the lattice parameters of the silicon nanowires and substrate respectively. According to Bragg's law at the first order: $2d\sin\theta = \lambda$, where θ is the diffraction angle. With the definition of the scattering vector $q = 4\pi/\lambda\sin\theta$, the lattice mismatch parameter can also be written: $\Delta a/a = (q_{Sub}-q_{SiNW})/q_{SiNW}$. As can be seen in Figure 4, $q_{SiNW} < q_{Sub}$, evidence that $\Delta a/a > 0$, and the lattice of the nanowires is in tension compared to the silicon substrate. This will be discussed later.

Figure 4 presents the results of diffraction profiles obtained by varying the incident angle close to the critical angle α_c. For short wires (S) and for α_i close to 0°, we observe only one peak (SiNW). As the angle of incidence α_i increases, a narrow peak of diffraction appears at the right of the (SiNW) peak. For $\alpha_i = \alpha_c$, this narrow peak becomes very marked, which can be attributed to the diffraction of the x-ray beam by the silicon substrate. As the wires are very short, when α_i increases, the cross section of the beam with the sample decreases and the intensity of (SiNW) decreases. The same phenomenon is also observed for $\alpha_i > \alpha_c$ (Figure 4

(b)). For long wires (L), Figure 4 (c) shows similar behaviour with the increase of the (Sub) intensity versus the increase of α_i. As the nanowires are long, the intensity of (SiNW) increases with α_i. For $\alpha_i > \alpha_c$, Figure 4 (d) reveals a slight decrease in the (Sub) intensity also due to the decrease in the cross section of the beam seen by the sample and is quantitatively plotted in Figure 5 for long wires (L). Similar measurements were performed out-of-plane along the (006) direction of the hexagonal system corresponding to the <111> direction of the silicon nanowires. For all the samples, the diffraction profiles reveal only one peak, evidence that $\Delta a/a_{<006>} \approx 0$. Consequently, no strain is measured along the direction of growth of the wires.

Figure 6 shows the evolution of the in-plane lattice mismatch parameter Δa/a versus the length of nanowires along the radial <300> direction (full circles). The in-plane $\Delta a/a$ is positive, corresponding to a small expansion of the crystalline lattice of SiNW. As can be seen, $\Delta a/a$ is close to $+5.2\times10^{-4}$ when the length of the wires $L > 1000$ nm, while for shorter nanowires, $\Delta a/a \approx +3.4\times10^{-4}$. The $\Delta a/a$ along the in-plane perpendicular direction was also measured and is indicated by full triangles. The values in both normal directions are very close and are in the experimental resolution range. Consequently, expansion is similar and the strain is symmetrical, in agreement with the symmetrical character of the cylindrical wires. In order to estimate the localization of the strains in the wires, we measured the in-plane $\Delta a/a$ along the <300> direction versus the incident angle $\alpha_i < \alpha_C$ (Figure 7). In this case, the sample is only probed by an evanescent wave. For both short (full circles) and long (full triangles) nanowires, $\Delta a/a$ decreases with α_i. The decrease is slight, but clearly visible and reproducible. This effect may have several origins. For instance, as $\Delta a/a$ is very small, the (SiNW) peak is very close to the narrow (Sub) peak of the substrate. It is known that a dynamical effect moves the (SiNW) peak away, which is contrary to observed measurements. Thus the observed displacement of the (SiNW) peak cannot be due to this effect. We believe

displacement is due more to the structure of the wires. Indeed, only a small part of the beam is coherent, and by varying the incident angle, the coherent part of the beam probes several parts of the wires. Clearly, for very small α_i values, the coherent part probes the top of the wires and, as α_i increases, the coherent part progressively probes the centre then the bottom of the wires. For the values of these angles, we clearly observe a decrease in the $\Delta a/a$ value. It appears that the in-plane $\Delta a/a$ is smaller closer to the bottom than the top of the nanowires, and is in agreement with the results for short wires shown in Figure 6.

In order to understand the origin of SiNW expansion, we performed measurements after removing the gold catalyst by dipping all the samples successively into the following solutions: HF, HNO_3-HCl, then HF again. Figure 8 presents the SEM images for medium (M) nanowires. The observation using secondary electrons (a) shows truncated nanowires where the Au/Si alloy head has disappeared. The silicon surface between wires is always clean. The samples were also observed in backscattering electron conditions (b), and no gold was observed at this scale. However, by increasing the resolution of the SEM, nanowires can be divided into two groups (Figure 9). A first group of wires (a) exhibits a head with a partially hemispherical crust shape. The head is composed of an alloy Au/Si. This head also exhibits an alloy layer at the head/body interface of the nanowire. Some small grains are visible on this crust. The facets of the wires are still clearly visible and do not appear modified after being dipped in the HNO_3-HCl solution. The observation in backscattering conditions (b) reveals the presence of small clusters with a high atomic number, which probably correspond to gold. These small clusters are particularly present on the silicon substrate surface as well as in the head alloy. A second group of nanowires (c) is composed of a head with only an alloy layer (thickness ≈ 40 nm). The observation in backscattering conditions (d) also shows the presence of very small gold grains. More accurately, although these grains may be 100% gold, they are more probably composed of an alloy, Au/Si. All samples were then investigated under x-ray

beam. XRR measurements (open circles Figure 3) always present the conventional total reflection plateau but not the thickness fringes observed previously with gold. Consequently, no gold is detected by XRR. GIXD measurements were performed with these samples and also revealed a Bragg diffraction peak (SiNW), as shown in Figure 10(a). The shape of the profile is similar to that obtained before with gold. The (Sub) peak is narrow and the (SiNW) peak slightly broader. By varying the incident angle α_i, we also observe the same behaviour with the increase in intensity before the critical angle. In order to compare both measurements before and after gold removal, we plotted two diffraction profiles (Figure 10(b)). The profile with the full circles corresponds to the sample with gold, while that with open circles corresponds to the sample without gold. We observe a small shift of the (SiNW) peak to the higher q values, corresponding to a small decrease in lattice expansion. This measurement was performed for all the samples and is plotted in Figure 6. The in-plane $\Delta a/a$ along the <300> direction is reported with open circles. We find a curve with a similar shape to that obtained with gold, with a small decrease in the in-plane $\Delta a/a$ for small nanowires (S). All values decrease by a constant $\approx 0.9\times10^{-4}$. Measurement along the perpendicular direction is reported with open triangles and reveals the same value. This again confirms the symmetrical character of the strain. Finally, we performed measurements of in-plane $\Delta a/a$ by varying the incident angle for $\alpha_i < \alpha_c$ (Figure 7 open circles and triangles). Once again, we observe a small shift in the $\Delta a/a$ value, confirming that $\Delta a/a$ is smaller closer to the substrate than to the top.

Let us now analyze the experimental strain in silicon nanowires. Many of the studies presented in the literature are theoretical predictions for very small nanostructures with a diameter $d < 10$ nm, for which the behaviour is significantly different from the bulk behaviour. At this scale, surface effects become strong and, more specifically, the surface to volume ratio

is high. One approach involves considering the strain of the entire volume of the particle, which means that the particle is fully compressed (positively or negatively) by the surface. This aspect has been investigated by Shuttelworth[17] who defined surface stress σ_{ii}^{surf} (N/m) by:

$$\sigma_{ij}^{surf} = \gamma\delta_{ij} + \frac{\partial\gamma}{\partial\varepsilon_{ij}} \quad \textbf{(1)}$$

where ε_{ij} is the strain produced by the change of surface energy γ (J/m^2). In the case of a liquid droplet, when the surface increases, its properties are invariant since atoms are transferred from the bulk to the surface, so that $\partial\gamma/\partial\varepsilon_{ij}$ = 0 and σ_{ii}^{surf} is always equal to the positive surface energy. In a solid, the positions of atoms are fixed, and an expansion of the surface modifies its properties so that surface stress σ_{ii}^{surf} is not equal to γ. In eq. (1), $\partial\gamma/\partial\varepsilon_{ij}$ can be either positive or negative. Usually, if $\partial\gamma/\partial\varepsilon_{ij}$ is not too large, σ_{ii}^{surf} is positive, corresponding to a compression. But if $\partial\gamma/\partial\varepsilon_{ij}$ is negative and large enough, σ_{ii}^{surf} can be negative corresponding to an expansion of the particle.[18] In the case of a cylindrical particle of diameter d and length l, we can consider the equilibrium of the hemi cylinder under 2 forces: a force $F_1 = \Delta Pdl$ due to the internal effective static pressure Δp, and the force $F_2 = \sigma_{ii}l$ exerted by the exposed edge of the surface of the cylinder. At the equilibrium $F_1 = F_2$, the following is obtained:

$$\sigma_{ii}^{surf} = Pd \quad \textbf{(2)}$$

Using the definition of the bulk modulus K, the effective static pressure can be written as: $\Delta P = -K(\Delta V / V_0)$. As previously suggested[19,20,21] in the case of a crystalline particle with a cubic structure with a lattice constant a, $\Delta V/V_0 = 3\Delta a/a$. Thus we have:

$$\sigma_{ii}^{surf} = -3\frac{\Delta a}{a}dK \quad \textbf{(3)}$$

For bulk hydrostatic loads, the bulk modulus K is usually expressed as: $K = E/(3(1-2\nu))$ where ν is the Poisson's ratio and E the Young's modulus. In the literature, ν is usually taken as a value close to $\nu = 0.28$[22, 23] or $\nu = 0.27$.[24] For E it is more complicated, as numerous values are found,[25, 26, 27, 28, 29] as shown in Table 1. The value for bulk Si varies from 120 GPa to 180 GPa. It is, however, usually accepted that E depends on the crystallographic orientation, for example, $E_{<100>}$ = 120-130 GPa. In the case of a <111> oriented crystal, the Young's modulus increases with $E_{<111>}$ = 149-185 GPa, which leads to K = 107-140 GPa. For small nanoparticles, contradictory results have been obtained, with E decreasing[29] or increasing[30] as the diameter decreases down to nanostructures. In our case, the mean diameter is around 185 nm but this value is an average between small nanostructures (a few nm) and large nanostructures (a few 100 nm). In these conditions, it is difficult to measure the influence of the size on the Young's modulus. Furthermore, A. San Paulo *et al.*[31] have shown that the Young's modulus for <111> silicon nanowires with diameters down to 100-200 nm is consistent with the bulk value. This is the reason why we take a mean value of E = 185 GPa. Finally, for the $\Delta a/a$ and d average value of 5.2×10^{-4} and d =185 nm respectively, and for K = 140 GPa, we find σ_{ii}^{surf} = -40 Nm^{-1}. This value is negative like that found for the small particles of silicon composing porous silicon (σ_{ii}^{surf} = -2 $N.m^{-1}$),[32] but it is far larger. This is not surprising because the system is quiet different. In the case of porous silicon, very small nanometric particles are inserted in a porous structure, whereas in the present case the shape of the particles is very cylindrical, with independent linear particles of quite large diameter. Furthermore, the present structures also contain gold catalyst. Although its influence is not completely clear, it must play a key role in the strain and stress of the silicon nanowires, as is shown in Figure 6. Finally, when gold is removed, the lattice mismatch parameter for long wires decreases from 5.2×10^{-4} to 4.3×10^{-4}, corresponding to a residual stress σ_{ii}^{surf} = -33 $Nm^{-}1$.

The measured strain is also evidence of the presence of bulk stress in the nanowires (Figure 11). In our case, we assume an in-plane strain of the wire. Under this condition, the problem is reduced to one of biaxial tension and the tensor is written as:

$$\begin{aligned} \sigma_x^{vol} &= \frac{E}{1-\nu^2}(\varepsilon_x + \nu\varepsilon_y) \\ \sigma_y^{vol} &= \frac{E}{1-\nu^2}(\varepsilon_y + \nu\varepsilon_x) \\ \sigma_z^{vol} &= 0 \end{aligned} \qquad \textbf{(4)}$$

In addition, we measure $\varepsilon_x \approx \varepsilon_y$ for all samples. This simplifies eq. (6) and we finally obtain:

$$\sigma_x^{vol} = \sigma_y^{vol} = \frac{(1+\nu)}{(1-\nu^2)} E\varepsilon_x \qquad \textbf{(5)}$$

For $\nu = 0.28$, $E_{<111>} = 185$GPa and $\Delta a/a = 5.2\times10^{-4}$, we find $\sigma_x^{vol} = \sigma_y^{vol} = 132$ MPa. This value is the stress which exists in a plane of a straight section of the silicon nanowire.

Finally, as suggested by D. Vanderbilt[33], the surface stress σ_{ii}^{surf} and the bulk stress $\sigma_{x,y}^{vol}$ can be related by the following tensor:

$$\sigma_{ij}^{surf} = \tfrac{1}{2} c \sigma_{ij}^{vol} \qquad \textbf{(6)}$$

where c is a lattice constant. With our values, we obtain c = -597 nm.

Let us now consider the origin of the positive strain observed in our case. Taking into account the nanometric size, this strain is probably due to surface effects from several origins. First of all, the size effect may play a role, but is probably only predominant if the diameter is less than 10 nm. Consequently, as our nanostructures have a diameter in the 30 nm-300 nm range, the size effect may be limited. These surface effects are more probably due to the surface cover, which leads to surface tension. Before removing the gold, the silicon nanowires were covered by a thin layer of native silicon oxide SiO_2. This is known to result in a small expansion of the lattice.[34] However, in the present case, the main influence on the strain is clearly the presence of gold, as we have demonstrated above. The migration of gold on the

silicon nanowire surface is a complicated phenomenon.[35] This phenomenon has also been the subject of a study using Transmission Electron Microscopy measurements[16] in which it was found that gold migration starts from the head of the wire and diffuses to the bottom on the external surface. They also show that this migration increases with an increase in growth temperature due to the increase in gold mobility. Furthermore, they show that gold migration also increases for low values of the partial pressure of silane during nanowire growth. Thus the migration of gold is often observed at the silicon nanowire surface, which is confirmed in the present study. In order to investigate the influence of gold on the positive value of $\Delta a/a$, we removed the gold hemispherical droplet from the wire head (and a little on the sides). This led to a small decrease in the lattice mismatch parameter. However, the $\Delta a/a$ did not decrease down to zero; there was a residual strain. What was the origin of this strain?

Careful observation of Figure 9 reveals that the gold has not been totally removed. Some Au/Si alloy clusters are still present on the sides, which may explain the residual strain. Furthermore, we believe that some Au/Si clusters are also present in the silicon nanowire volume. To our knowledge, this aspect has never been examined before in the literature, but from our measurements it seems very probable that some gold clusters are present in the volume. Finally, surface effects, after gold removal, may also come from the Si-H bonds that are usually present on a silicon surface after dipping the sample in an acid HF solution. Earlier studies[32] have observed that these Si-H bonds lead to a small expansion of the silicon, whereas the natural state of silicon is to be compressed without the presence of Si-H bonds.[36] This phenomenon probably plays a key role in the expansion of the present wires. A more detailed study must be undertaken to clarify this aspect.

In summary, a small in-plane positive lattice mismatch parameter $\Delta a/a$ of a few 10^{-4} between silicon nanowires and a bulk silicon substrate was experimentally measured by GIXD, and was found to correspond to a small in-plane expansion of the nanowires (i.e. along and normal to the <300> direction). Measurements were also performed out-of-plane (i.e. along the

<006> direction) but no strain was found. It was revealed that this small strain was more pronounced at the top of the wire than at the bottom, which is close to the substrate. In all cases, the strain, although quite weak, was able to be accurately measured. Some possible origins of this expansion have been suggested. The influence of the gold catalyst was measured and the results presented, but other origins are suggested such as the presence of Si-H bonds on the nanowire surface.

Experimental

Silicon Nanowires were grown on a standard *p*-type silicon wafer, <111> oriented and highly boron-doped with a resistivity of about 0.01 Ωcm. Gold catalyst was firstly evaporated on the silicon wafer in a Physical-Vapour-Deposition (PVD) reactor, resulting in a thin gold layer of 2 nm thick. Samples were then annealed, consequently the equilibrium of this gold layer changes and there is a 2D-3D transition leading to the dewetting of the layer. The dewetting results in hemi spherically shaped droplets, the diameters of which present a distribution from 30 nm up to 300 nm. The droplets are randomly and homogeneously dispersed all over the surface of the silicon wafer. The sample surface was prepared with a preliminary annealing at T = 850°C during 10 min under a gaseous dihydrogen (H_2) flow. Catalytic growth of silicon nanowires was performed in a Chemical Vapour Deposition (CVD) reactor using the Vapour Liquid Solid (VLS) method. The gaseous precursor was silane (SiH_4) (partial pressure 20 mbar) while the carrier gas was dihydrogen (H_2). Gold removal was obtained by using the following procedure: the samples were dipped in a Hydrofluoric acid (HF) 1% solution, then in a mixture of Nitric acid (HNO_3) and Hydrochloric acid (HCl) [3:1], and finally again in a HF 1% acid solution. Scanning Electron Microscopy (SEM) images were performed using a Zeiss apparatus with a Gemini column with a field effect filament leading to nanometric resolution in the images. The x-ray measurements were performed at the European Synchrotron Radiation Facility (ESRF) in Grenoble (France) with the BM2 beamline. The

selected energy was E = 11.4 keV corresponding to a wavelength λ = 0.108758 nm. The experimental set-up was a 7-circle goniometer, and the detector was a punctual NaI scintillator. All the measurements were performed at room temperature and under atmospheric pressure.

Acknowledgements

We sincerely thank P. Ferret for help during Si nanowire growth, the BM2 beamline staff during experiments and F. Oehler for fruitful discussion.

Received: ((will be filled in by the editorial staff))
Revised: ((will be filled in by the editorial staff))
Published online: ((will be filled in by the editorial staff))

[1] R. Yan, D. Gargas, P. Yang, Nature Photonics Vol 3 (October 2009).

[2] R.S. Wagner, W.C. Ellis, Appl. Phys. Lett. **4** 89 (1964).

[3] O. Demichel, F. Oehler, V. Calvo, P.Noe, N. Pauc, P. Gentile, P. Ferret, T.Baron, N. Magnea, *Physica E 41 963 (2009).*

[4] P. Biagioni, M. Celebrano, M. Savoini, G. Grancini, D. Brida, S. Mátéfi-Tempfli, M. Mátéfi-Tempfli, L. Duò, B. Hecht, G. Cerullo, M. Finazzi, *Phys. Rev. B 80, 045411 (2009).*

[5] A. Sandhu, *Nature Nanotechnology* (1 May 2009).

[6] Z. Fan, H. Razavi, J-W Do, A. Moriwaki, O. Ergen, Y-L Chueh, P. W. Leu, J. C. Ho, T. Takahashi, L. A. Reichertz, S. Neale, K. Yu, M. Wu, J. W. Ager, A. Javey, *Nature Materials Vol 8 August (2009).*

[7] Y. Dong, B. Tian, T. J. Kempa, C.M. Lieber, *Nanoletters **9** 2183 (2009).*

[8] M. Jeon, K. Kamisako, *Materials Letters 63 777 (2009)*

[9] V. Sivakov, A.G. Gawlik, A. Berger, J. Plentz, F. Falk, S. H. Christiansen, *Nanoletters* ***9*** *1549 (2009).*

[10] V. Favre-Nicolin, J. Eymery, R. Koester, P. Gentile, Phys. Rev. B **79** 195401 (2009).

[11] T. Takeuchi, K. Tatsumura, T. Shimura, I. Ohdomari, J. Appl. Phys. **106** 073506 (2009).

[12] Z. Yang, Z. Lu, Y.P. Zaho, J. Appl. Phys. **106** 023537 (2009).

[13] R. Rurali, A. Poissier, N. Lorente, Phys. Rev. B **74** 165324 (2006).

[14] F.M. Ross, J. Tersoff, M.C. Reuter, Phys. Rev. Lett. **95** 146104 (2005).

[15] T. David, D. Buttard, T. Schülli, F. Dallhuin, P. Gentile, Surf. Science **602** 2675 (2008).

[16] M.I den Hertog, J.L. Rouvière, F. Dhalluin, P.J. Desré, P. Gentile, P. Ferret, F. Oelher, T. Baron, Nano Lett. **8** 1544 (2008).

[17] R. Shuttelworth, Proc. Phys. Soc. **A 63** 444 (1950).

[18] M.B. Webb, Surf. Science **299/300** 454 (1994).

[19] H.J. Wassermann, J.S. Vermaak, Surf. Science **22** 164 (1970).

[20] J.S. Vermaak, C.W. Mays, D. Kuhlmann-Wilsdorf, Surf. Science **12** 128 (1968).

[21] C.W. Mays, J.S. Vermaak, D. Kuhlmann-Wilsdorf, Surf. Science **12** 134 (1968).

[22] H.J. McSkimin, J. Appl. Phys. **24** 988 (1953).

[23] H.J. McSkimin, P. Andreatch J. Appl. Phys. **35** 2161 (1964).

[24] B. Lee, R. E. Rudd, Phys. Rev. B **75** 195328 (2007).

[25] D. Bellet, P. Lamagnère, A. Vincent, Y. Brechet, *J. Appl ; Phys.* **80** 3772 (1996).

[26] Y. Umeno, A. Kushima, T. Kitamura, P. Gumbsch, J. Li, Phys.Rev. B **72** 165431 (2005).

[27] M. Tabib-Azar, M. Nassirou, R. Wang, Appl. Phys. Lett. **87** 113102 (2005).

[28] P. Hess, Appl. Surf. Sci. **106** 429 (1996).

[29] M. Menon, D. Srivastava, I. Ponomareva, L.A. Chernozatonskii, Phys. Rev. B **70** 125313 (2004).

[30] M.J. Gordon, T. Baron, F. Dhalluin, P. Gentile, P. Ferret, Nano Lett. **9** 525 (2009).

[31] A. San Paulo, J. Bokor, R.T. Howe, R. He, P. Yang, D. Gao, C. Carraro, R. Maboudian, Appl. Phys. Lett. 87 053111 (2005).

[32] D. Buttard, G. Dolino, C. Faivre, A. Halimaoui, F. Comin, V. Formoso, L. Ortega J. Appl. Phys. **85** 7105 (1999).

[33] D. Vanderbilt, Phys. Rev. Lett. **59** 1456 (1987).

[34] D. Buttard, D. Bellet, G. Dolino, J. Appl. Phys. **79** 8060 (1996).

[35] J.B. Hannon, S. Kodambaka, F.M. Ross, R.M. Tromp, Nature **440** 69 (2006).

[36] R.Q. Zhang Y. Lifshitz, D.D.D Ma, Y.L. Zhao, T. Frauenheim, S.T. Lee, S. Y. Tong, J. Chem. Phys. **123** 144703 (2005).

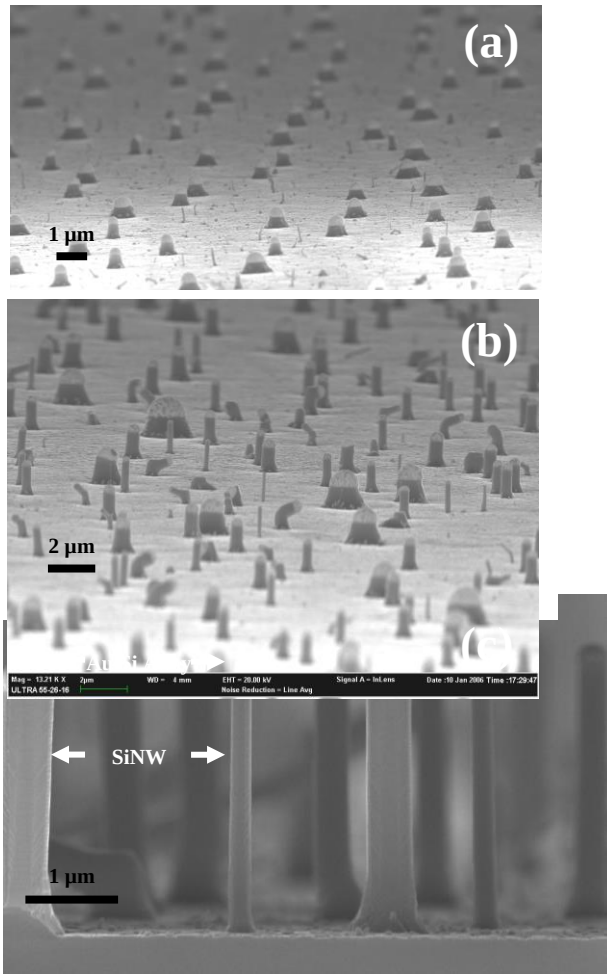

Figure 1
SEM images from Silicon nanowires (SiNW) grown using VLS method for three growth conditions: (a) $t = 10$ min at $T = 650°C$ and 5 sccm of Silane (SiH_4) "short" wires (S), (b) $t = 15$ min at $T = 700°C$ and 10 sccm of Silane, $L = 1177$ nm "medium" wires (M), (c) $t = 15$ min at $T = 575°C$ and 10 sccm of Silane $L = 2782$ nm "long" wires (L).

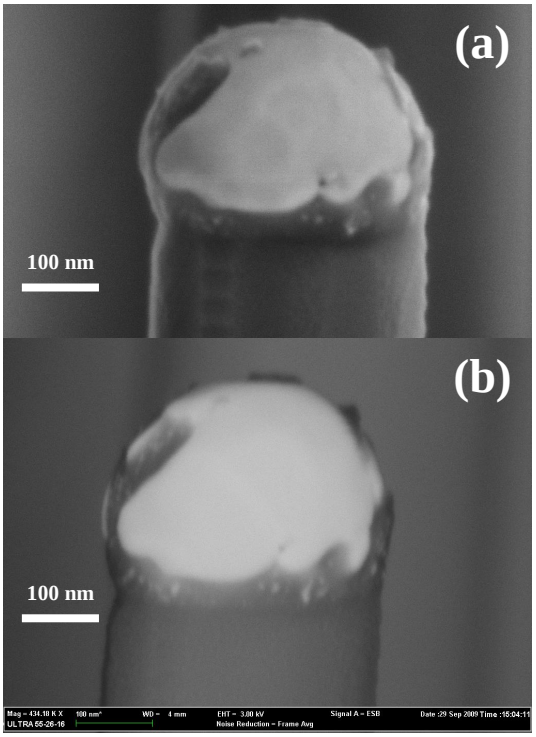

Figure 2

Details from SiNW head with several zones in the Au/Si alloy: (a) view in topographic mode, (b) view in chemical contrast mode, showing evidence of two parts in the alloy: rich and poor in Au.

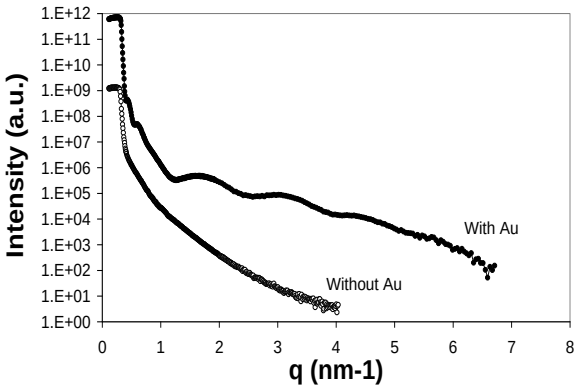

Figure 3
XRR profiles from SiNW samples with gold (dark circles) and without gold (open circles). The reflected intensity is plotted in arbitrary units versus the scattering vector *q*. The oscillations are evidence of the presence of gold particles.

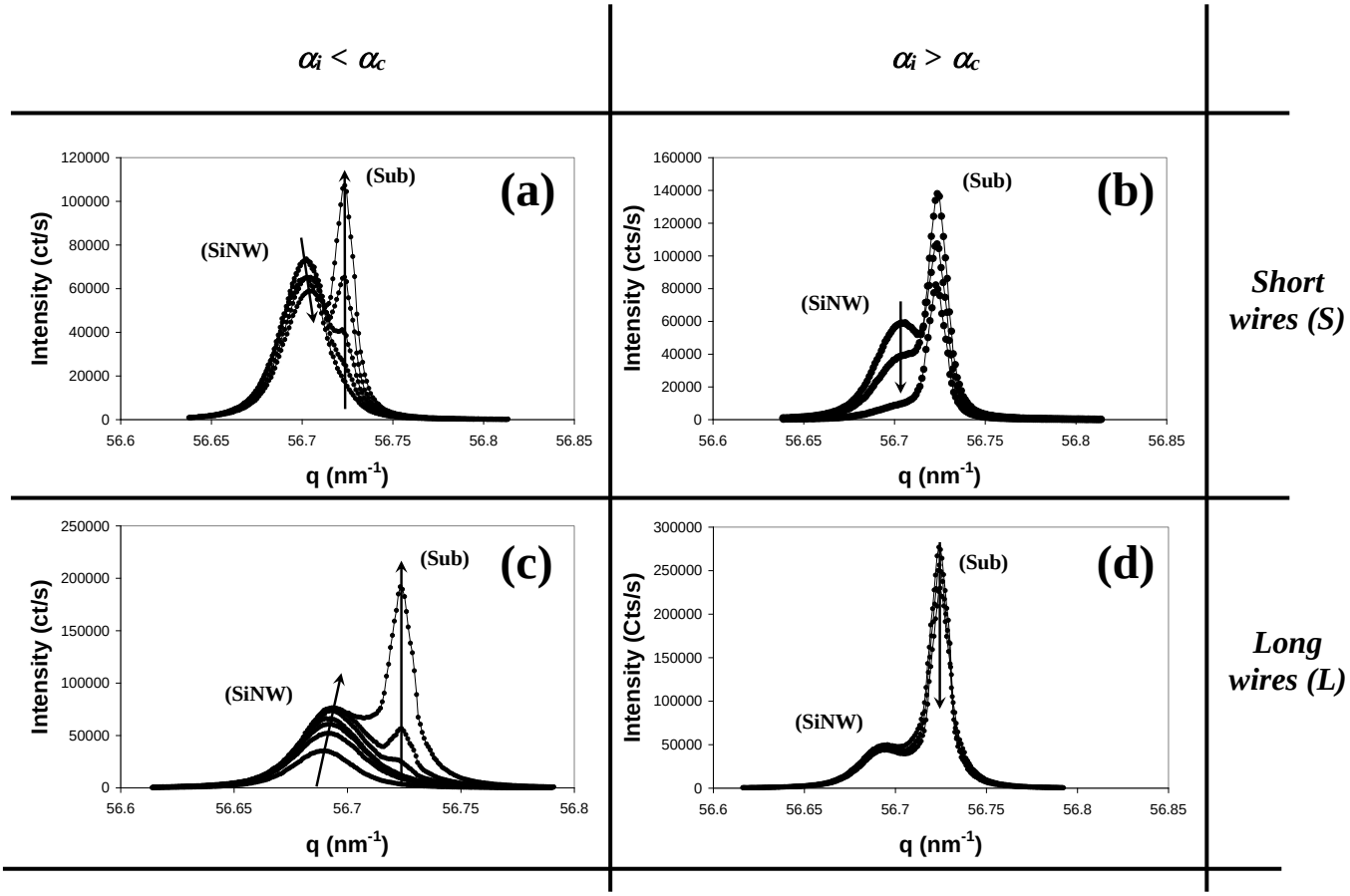

Figure 4
GIXD profiles from the diffraction by <111> SiNW samples with the gold catalyst along the <300> direction of the hexagonal system (i.e. in the direction normal to the wires in the plane of the sample). (Sub) and (SiNW) are Bragg's peaks of diffraction respectively by the silicon substrate and the Silicon nanowires. Diffracted intensity is plotted versus the scattering vector *q*.

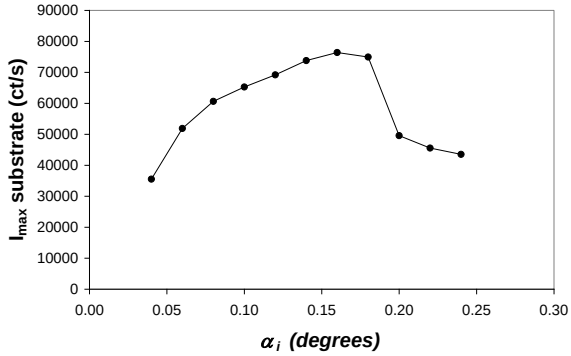

Figure 5
Absolute value of the intensity of the peak (Sub) versus the incidence angle α_i.

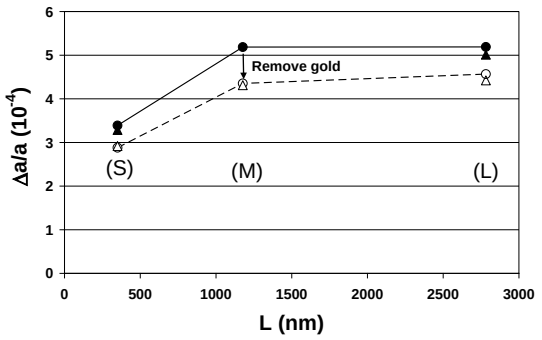

Figure 6
In-plane lattice mismatch parameter ($\Delta a/a$) between the SiNW and the silicon substrate for three lengths of wire, referred to as "Short" (S), "Medium" (M) and "Long" (L), along the <300> direction (circles) and normal to the <300> direction (triangles). The dark marks (respectively open) correspond to nanowires with gold (respectively without gold).

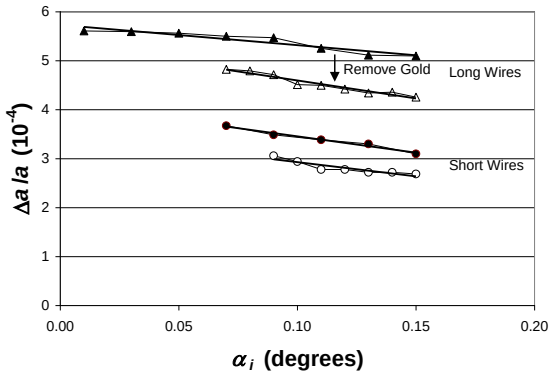

Figure 7
In-plane lattice mismatch parameter ($\Delta a/a$) between the SiNW and the silicon substrate versus the incidence angle α_i. Dark marks correspond to nanowires with gold catalyst and the open ones correspond to the wires without gold catalyst.

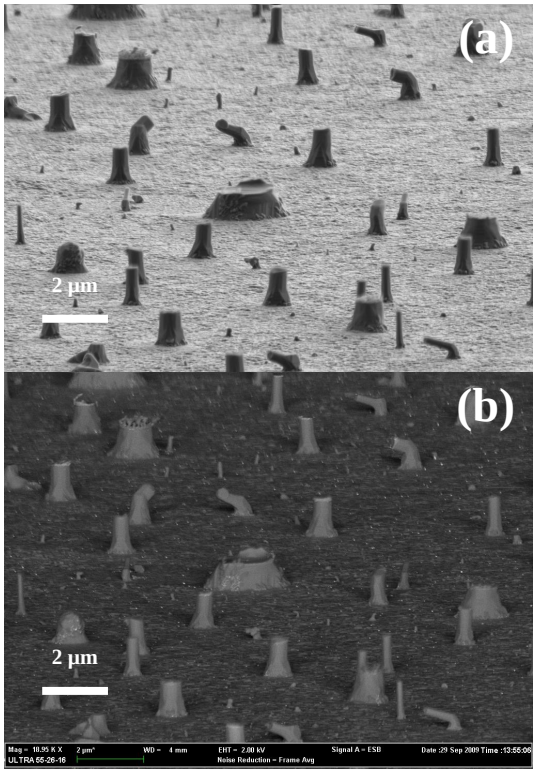

Figure 8
SEM images from Medium (M) wires after removing gold catalyst: (a) in secondary electrons mode and (b) in backscattered mode.

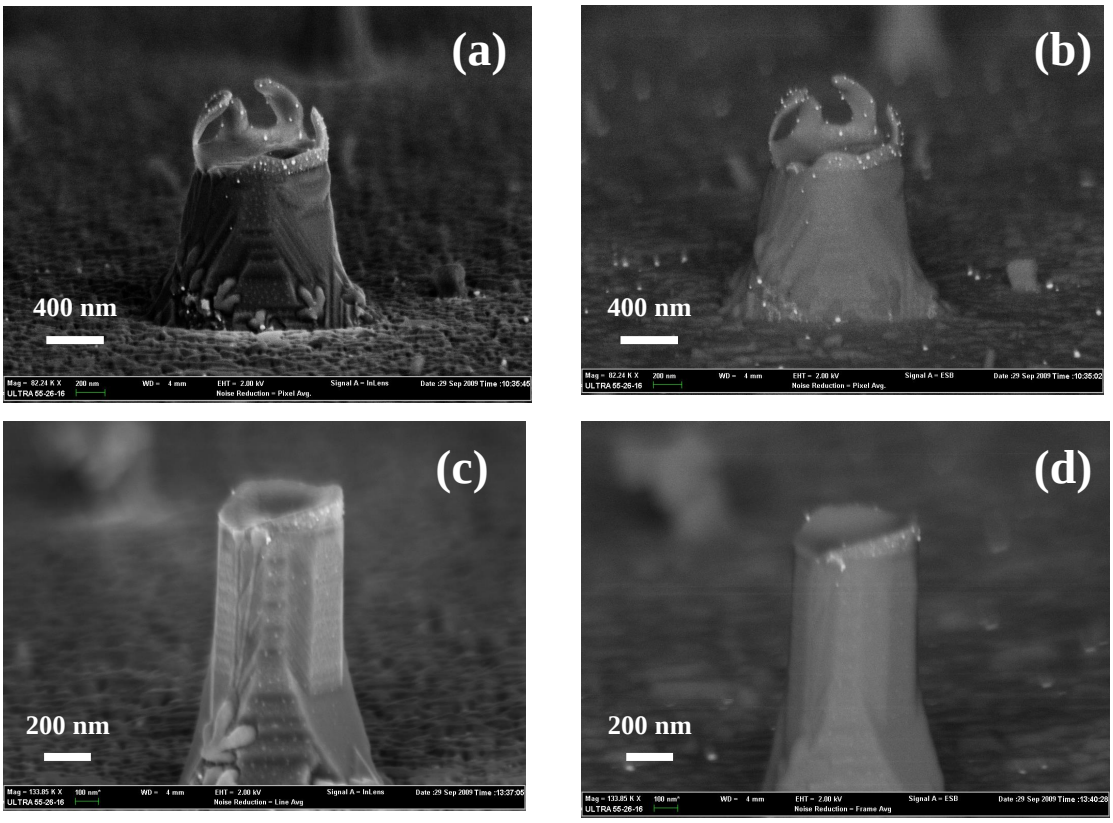

Figure 9
Details of wires after removal of the gold catalyst. Two typical populations are observed: (a) the head of the wires is composed of an alloy crust Au/Si with an underlayer, and (c) the head is only composed of an underlayer of an alloy Au/Si. Images (b) and (d) are the corresponding observations using backscattered electrons signal.

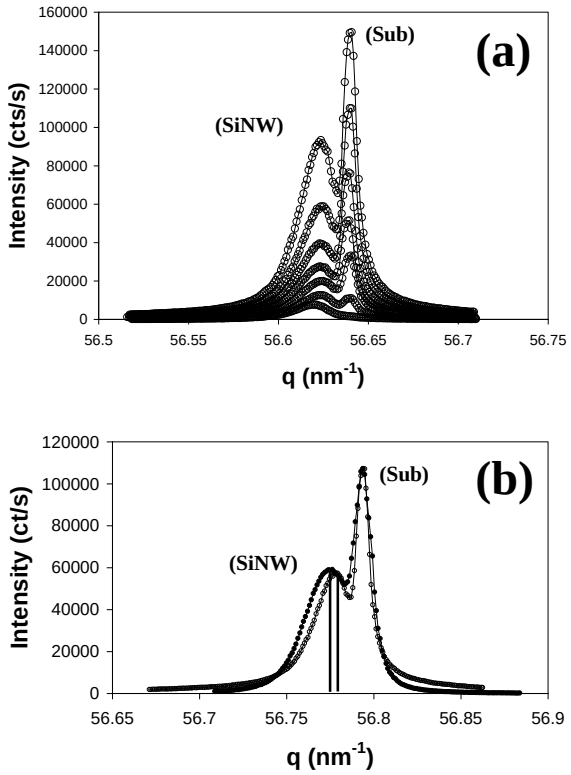

Figure 10
(a) GIXD profiles for long wires (L) after the removal of the gold catalyst. (b) Comparison of two typical profiles of diffraction before and after the removal of gold.

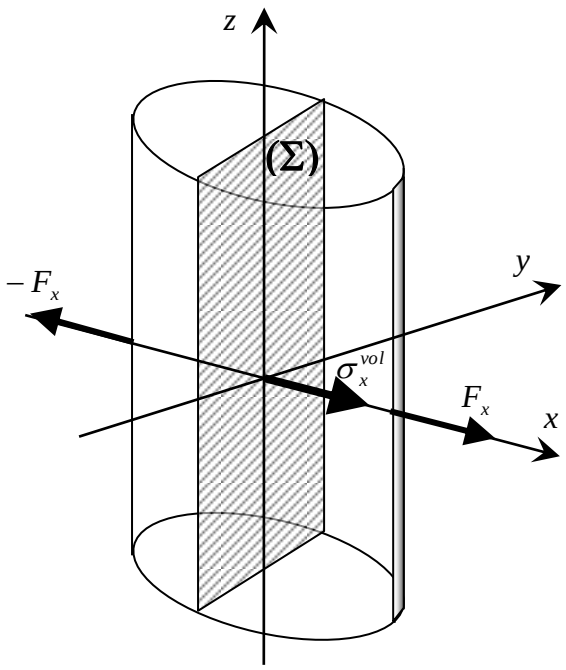

Figure 11
Schematic representation of a plane biaxial expansion of a cylinder. σ_x^{vol} is the normal stress applied on the section Σ.

Table 1
Young's modulus *E* and Poisson's ratio ν from several references along three crystallographic directions. *Experimental, **Calculations.

Reference	Direction	$E_{Si\ bulk}$ (GPa)	E_{Sinw} *(GPa)*	ν
*D. Bellet *et al.* [25]	<100>	120	-	-
*M.J. Gordon *et al.* [30]	<100>	130	-	-
	169	-	-	
	<111>	185	100-180	-
**B. Lee *et al.* [24]	<100>	122.8	-	0.27
**Y.Umeno *et al.* [26]	<100>	125.1	-	0.26
*H.J. McSkimin [22]	<100>	131.4	-	0.28
*Tabib-Azar *et al.* [27]	<111>	185	93-250	-
*P. Hess [28]	<111>	160	-	0.27
**Menon *et al.* [29]	<111>	149	147 (*Tetrahedral*)	0.25
	<111>	-	94 (*Cagelike*)	-